

# Optical spectroscopic characterization of *Fermi* blazar candidates of uncertain type with TNG and DOT: First Results

Amanda Olmo-García,<sup>1,2</sup> Vaidehi S. Paliya,<sup>3</sup>★ Nuria Álvarez Crespo<sup>2,4</sup>† Brajesh Kumar,<sup>5</sup>

Alberto Domínguez,<sup>2,4</sup> Armando Gil de Paz<sup>1,2</sup> and Patricia Sánchez-Blázquez<sup>1,2</sup>

<sup>1</sup>Departamento de Física de la Tierra y Astrofísica, Universidad Complutense de Madrid, E-28040 Madrid, Spain

<sup>2</sup>Instituto de Física de Partículas y del Cosmos (IPARCOS), Universidad Complutense de Madrid, E-28040 Madrid, Spain

<sup>3</sup>Inter-University Centre for Astronomy and Astrophysics (IUCAA), SPPU Campus, 411007, Pune, India

<sup>4</sup>Departamento de Estructura de la Materia, Física Térmica y Electrónica, Universidad Complutense de Madrid, E-28040 Madrid, Spain

<sup>5</sup>Aryabhata Research Institute of Observational Sciences (ARIES), Manora Peak, Nainital 263001, India

Accepted XXX. Received YYY; in original form ZZZ

## ABSTRACT

The classification of  $\gamma$ -ray-detected blazar candidates of uncertain type (BCU) is a relevant problem in extragalactic  $\gamma$ -ray astronomy. Here we report the optical spectroscopic characterization, using two 3–4 m class telescopes, Telescopio Nazionale Galileo and Devasthal Optical Telescope, of 27 BCUs detected with the *Fermi* Large Area Telescope. Since the identification of emission lines is easier in broad-line blazars, which usually exhibit low frequency peaked (synchrotron peak frequency  $\leq 10^{14}$  Hz) spectral energy distribution, we primarily target such BCUs. We found that 8 out of 27 sources exhibit broad emission lines in their optical spectra, 3 of them have redshifts  $>1$  and the farthest one is at  $z = 2.55$ . The optical spectra of 2 of the 19 remaining objects are dominated by the absorption spectra of the host galaxy, and there is a tentative detection of the Lyman- $\alpha$  absorption feature in one source. The spectra of the remaining 16 objects, on the other hand, are found to be featureless.

**Key words:** galaxies: active – gamma-ray: galaxies – BL Lacertae objects: general

## 1 INTRODUCTION

The Large Area Telescope (LAT) onboard the *Fermi Gamma-ray Space Telescope* has detected thousands of extragalactic objects in high-energy  $\gamma$ -rays (Abdollahi et al. 2020). The majority of them ( $>90\%$ ) are blazars, an extreme class of active galactic nuclei (AGN) with relativistic jets aligned close to the line of sight to the observer (Ajello et al. 2020). Blazars are distinguished into two classes: BL Lac objects having emission lines in their optical spectra with rest-frame equivalent width  $EW \leq 5 \text{ \AA}$ , and Flat Spectrum Radio Quasars (FSRQs,  $EW > 5 \text{ \AA}$ ), showing optical features as in normal quasar spectra (Stickel et al. 1991). The broadband spectral energy distribution (SED) of blazars shows a typical double-peaked structure with the lower energy peak explained by the synchrotron process and the high-energy emission originating via the inverse Compton mechanism. FSRQs generally exhibit low frequency peaked SEDs (synchrotron peak frequency  $\nu_{\text{syn}}^{\text{peak}} \lesssim 10^{14}$  Hz), whereas BL Lacs typically peak at higher frequencies ( $\nu_{\text{syn}}^{\text{peak}} > 10^{15}$  Hz, Ajello et al. 2020).

There are  $\sim 30$  per cent of *Fermi*-LAT detected sources that exhibit multi-frequency behavior similar to blazars (e.g., flat radio spectra), but often no optical spectra are available to identify their class (FSRQ/BL Lacs) or their signal-to-noise ratio is too low for a precise determination of their nature. Such objects are termed as blazar can-

didates of uncertain type (BCUs, e.g., Ackermann et al. 2011). There have been various methods developed to properly assess the physical properties of BCUs and classify them, e.g., based on their location in the WISE color-color diagram where  $\gamma$ -ray emitting blazars occupy a distinct place (Massaro et al. 2012) and machine learning algorithms (cf. Doert & Errando 2014; Kang et al. 2019; Kovačević et al. 2020; Chiaro et al. 2021). However, none of these methods offer a conclusive way to clarify the nature of BCUs, unless there is an optical spectroscopic confirmation. Various optical spectroscopic followup campaigns have been organized to address this problem (e.g., Paggi et al. 2014; Massaro et al. 2015; Landoni et al. 2015; Álvarez Crespo et al. 2016; Klindt et al. 2017; Paiano et al. 2017; Marchesi et al. 2018; Desai et al. 2019a; Marchesini et al. 2019; Peña-Herazo et al. 2019; Paiano et al. 2019; Paliya et al. 2020c; Rajagopal et al. 2021).

The classification of BCUs is crucial to (1) improve the completeness of *Fermi*-LAT catalogs, (2) build the luminosity function of blazars (Ajello et al. 2012), (3) select potential targets for the Cherenkov Telescope Array (e.g., Sol et al. 2013; Hassan et al. 2017; Paiano et al. 2021), (4) study emission mechanisms and physical properties (e.g., Paliya et al. 2017, 2020a, 2021), (5) obtain stringent limits on the extragalactic background light (e.g., *Fermi*-LAT Collaboration et al. 2018; Desai et al. 2019b; Franceschini et al. 2019; Saldana-Lopez et al. 2021), including constraints on the Hubble constant (Domínguez et al. 2019), (6) search for counterparts of new flaring  $\gamma$ -ray sources (Bernieri et al. 2013; Pasham & Wevers 2019), (7) test new  $\gamma$ -ray detection algorithms (cf. Campana et al. 2015), (8) discover the new subclass of  $\gamma$ -ray emitting sources, such as radio weak or extreme BL Lacs (Massaro et al. 2017; Nievas

★ E-mail: vaidehi.s.paliya@gmail.com (VSP)

† E-mail: nalvarezcrespo@ucm.es (NAC)

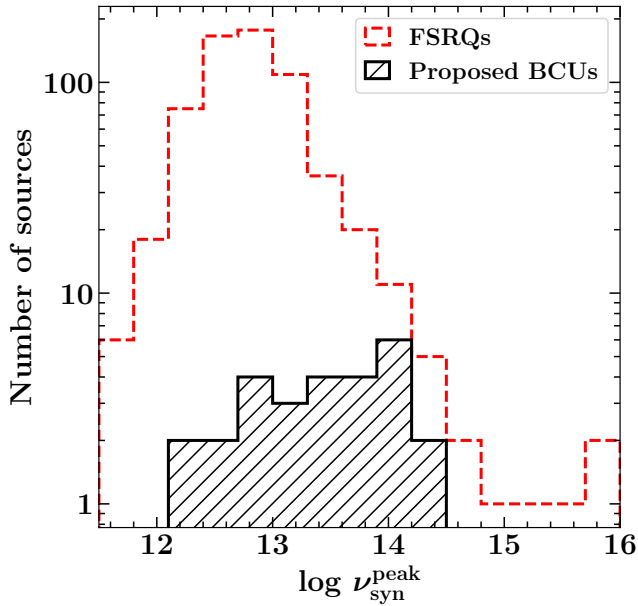


**Figure 1.** Distributions of the synchrotron peak frequencies.

Rosillo et al. 2022), and (9) search for electromagnetic counterparts of IceCube detected neutrinos (e.g., Paliya et al. 2020b).

Motivated by the above-mentioned science problems, we have started an optical spectroscopic follow-up campaign to secure optical spectra of reasonably bright *Fermi*-BCUs with medium 3-4 m class telescopes. In this paper, we present the results obtained for 27 blazars using observations taken with 3.6 m Telescopio Nazionale Galileo (TNG) located at the Roque de Los Muchachos Observatory on the island of La Palma in the Canary Islands, Spain, and Devasthal Optical Telescope (DOT) located at the Devasthal Observatory, Nainital, India. It is a well-known fact that FSRQs exhibit broad emission lines which are easier to identify in relatively short exposure observations. Therefore, to identify potential FSRQs among the sample of BCUs, we prioritized sources with  $\nu_{\text{syn}}^{\text{peak}} < 10^{14}$  Hz. This is because broad emission line blazars or FSRQs are usually low synchrotron peaked (LSP) sources (Ackermann et al. 2011), though some BL Lac sources could also exhibit LSP SEDs. This is shown in Figure 1. Additionally, we also observed BL Lac 4FGL J1330.4+3157, associated with the radio source CGRaBS J1329+3154, which is reported to be a  $z = 3.79$  quasar based on its low signal-to-noise spectrum taken with the Sloan Digital Sky Survey (Lyke et al. 2020), to ascertain its spectroscopic redshift. We describe the sample selection in Section 2 and provide steps of data reduction in Section 3. The results are presented in Section 4 followed by a brief description of individual BCUs in Section 5. We summarize our findings in Section 6.

## 2 SAMPLE SELECTION

The second data release of the fourth catalog of the *Fermi* LAT detected AGN (4LAC-DR2; Ajello et al. 2020) contains 1499 BCUs including 1292 blazars with no redshift information. All of them have low-frequency, usually radio, counterparts reported in 4LAC-DR2. The association of a  $\gamma$ -ray emitter with a radio/optical/X-ray source is usually done following statistical methods as adopted in *Fermi*-LAT catalogs (cf. Ajello et al. 2020). For example, the like-

likelihood ratio association technique (Mattox et al. 1996; Ackermann et al. 2011) considers several surveys, e.g., NRAO VLA Sky Survey (NVSS, Condon et al. 1998) and the ROSAT All Sky Survey (Voges et al. 1999), and estimates the probability that a candidate is a ‘true’ counterpart. The angular separation and brightness of radio sources lying within the considered uncertainty region of the  $\gamma$ -ray source are taken into account while deriving the association probability. For a probability value  $>80\%$ , an object is considered as a high-confidence counterpart of the  $\gamma$ -ray source (see, further details in Ackermann et al. 2011).

We selected blazars which were visible from the TNG ( $28^{\circ}45'14.4''\text{N}$ ,  $17^{\circ}53'17.3''\text{W}$ ) and the DOT ( $29^{\circ}21'40''\text{N}$ ;  $79^{\circ}41'04''\text{E}$ ) and having *R*-band magnitude  $< 20$  mag. At TNG, we were granted 4.5, 1.5 and 4.5 nights during cycle 2020B (January 9-13, 2021), 2021A (July 2-3, 2021) and 2021B (December 6-10, 2021), respectively. Additionally, we were allocated half service night at TNG (May 22, 2021). Due to bad weather, 4 of the allocated 4.5 nights and 2.5 of the allocated 4.5 nights in cycle 2020B and 2021B, respectively, were lost. On DOT, we were awarded one night in the 2021-C1 cycle. Altogether, we were able to acquire optical spectra of 27 *Fermi*-BCUs. The general properties of these objects are provided in Table 1.

## 3 OBSERVATIONS AND DATA REDUCTION

### 3.1 Telescopio Nazionale Galileo (TNG)

We used the spectrograph DOLORES (Device Optimized for the LOw RESolution) to take optical spectra of *Fermi*-BCUs with TNG. We used the LR-B grism and the 1 arcsec slit, which gives a spectral resolution  $R = 585$ , and a reciprocal dispersion of  $2.52 \text{ \AA pixel}^{-1}$  in the wavelength range 3000 to 8430  $\text{\AA}$ . The slit was oriented at the parallactic angle. The total integration time was divided into exposures of 20 minutes as a compromise between signal-to-noise and contamination from cosmic rays. The total integration time for each object is listed in Table 1.

### 3.2 Devasthal Optical Telescope (DOT)

We used the low resolution slit-spectrograph ARIES Devasthal Faint Object Spectrograph & Camera (ADFOSC) mounted at the 3.6 m DOT. The spectral dispersions provided by the different gratings are in the range of 1 to 7  $\text{\AA pixel}^{-1}$  and an 8' long slit with different available widths (0.4''–3.2'') can be used. The spectra cover the wavelength range 3500-10500  $\text{\AA}$  with a spectral resolution  $R = 515$ . Further details about the instrument can be found in Omar et al. (2012). We observed 5 *Fermi*-BCUs with ADFOSC on the night of March 21, 2021 (Table 1).

### 3.3 Data Reduction

The reduction of the spectra was done following the standard procedure with IRAF<sup>1</sup> tasks, through the PyRAF software<sup>2</sup>. The initial

<sup>1</sup> <http://iraf.noao.edu/> IRAF is distributed by the National Optical Astronomy Observatory, which is operated by the Association of Universities for Research in Astronomy (AURA) under cooperative agreement with the National Science Foundation.

<sup>2</sup> PyRAF is a product of the Space Telescope Science Institute, which is operated by AURA for NASA <http://www.stsci.edu/institute/softwarehardware/pyraf/>

**Table 1.** The list of the  $\gamma$ -ray detected BCUs monitored in this work. Column information are as follows: (1) 4FGL source name; (2) other name; (3) right ascension (J2000); (4) declination (J2000); (5) apparent  $R$ -band magnitude; (6) Galactic extinction ( $E(B - V)$ ) in mag; (7) date of observation (yyyy/mm/dd); (8) telescope used; (9) exposure time, in seconds; and (10) mean signal-to-noise ratio of the spectrum.

4FGL Name (1)	Assoc. Name (2)	RA (J2000) (3)	Decl. (J2000) (4)	$R$ mag. (5)	$E(B - V)^a$ (6)	Date (7)	Telescope (8)	Exposure (9)	S/N (10)
J0024.4+4647	B3 0021+464	00 24 21.54	+46 44 06.2	19.07	0.07	2021/12/10	TNG	3600	18
J0028.9+3553	GB6 J0028+3550	00 28 51.97	+35 50 36.1	18.35	0.06	2021/01/13	TNG	2400	11
J0130.6+1844	MG1 J013030+1843	01 30 30.65	+18 43 21.9	19.56	0.05	2021/12/09	TNG	5400	8
J0223.5+3912	B3 0220+390	02 23 28.40	+39 12 51.3	18.51	0.05	2021/12/10	TNG	2400	48
J0233.5+0654	TXS 0230+067	02 33 29.99	+06 55 26.4	18.76	0.11	2021/01/13	TNG	2400	10
J0244.7+1316	GB6 J0244+1320	02 44 45.69	+13 20 07.2	18.91	0.09	2021/01/13	TNG	2400	9
J0421.0-0752	PKS 0418-079	04 20 53.94	-07 52 19.9	18.49	0.09	2021/12/09	TNG	2400	18
J0430.3+1654	MG1 J043022+1655	04 30 22.35	+16 55 04.7	18.79	0.32	2021/01/13	TNG	2400	11
J0526.3+2246	NVSS J052622+224801	05 26 22.03	+22 48 02.1	19.31	0.56	2021/12/09	TNG	3600	6
J0604.9+0000	GB6 J0604+0000	06 04 58.42	+00 00 43.2	16.04	0.50	2021/12/09	TNG	1200	43
J0638.2+6020	GB6 J0638+6016	06 38 35.75	+60 17 03.0	18.53	0.07	2021/12/09	TNG	2400	13
J0704.7+4508	B3 0701+451	07 04 50.97	+45 02 41.8	18.50	0.09	2021/01/13	TNG	2400	16
J0746.5-0710	PMN J0746-0709	07 46 27.49	-07 09 49.6	18.87	0.10	2021/03/21	DOT	5400	7
J0749.6+1324	GB6 B0746+1329	07 49 35.95	+13 21 56.0	19.45	0.03	2021/12/10	TNG	4800	2
J0804.5+0414	TXS 0802+043	08 04 43.52	+04 14 10.0	18.41	0.02	2021/12/10	TNG	2400	19
J0929.6+4621	GB6 B0926+4634	09 29 22.76	+46 20 46.5	18.08	0.02	2021/12/09-10	TNG	2400	9
J0959.6+4606	2MASX J09591976+4603515	09 59 19.81	+46 03 51.9	18.06	0.01	2021/03/21	DOT	2400	19
J1118.2-0415	PMN J1118-0413	11 18 12.46	-04 13 24.4	19.15	0.04	2021/03/21	DOT	6000	21
J1129.2-0529	NVSS J112914-052856	11 29 14.06	-05 28 56.3	18.68	0.04	2021/05/22	TNG	2400	21
J1330.4+3157	CGRaBS J1329+3154	13 29 52.87	+31 54 11.06	20.00	0.01	2022/04/19	TNG	5400	7
J1419.4-0838	NVSS J141922-083830	14 19 22.56	-08 38 32.1	18.13	0.04	2021/03/21	DOT	3600	12
J1549.3+6310	WN B1549+6319	15 49 57.32	+63 10 07.3	17.75	0.02	2021/05/22	TNG	1200	9
J1756.9+1531	87GB 175437.6+153548	17 56 53.10	+15 35 20.8	19.36	0.09	2021/07/03	TNG	3600	11
J1822.0+1600	OU 134	18 22 09.97	+16 00 14.8	18.59	0.17	2021/07/02	TNG	3600	39
J1836.5+1948	NVSS J183632+195047	18 36 32.11	+19 50 46.3	19.33	0.22	2021/07/02	TNG	3600	22
J1845.0+1613	87GB 184225.9+161105	18 44 42.61	+16 14 11.1	17.93	0.40	2021/07/02	TNG	2400	21
J1949.0+1314	87GB 194635.4+130713	19 48 55.22	+13 14 39.9	19.00	0.24	2021/07/03	TNG	3600	29

NOTE — <sup>a</sup> Average reddening value by Schlafly & Finkbeiner (2011), obtained from <https://irsa.ipac.caltech.edu/applications/DUST/>.

steps are: bias subtraction, flat correction, cosmic ray removal (van Dokkum 2001) and wavelength calibration. Flats were not available in the data from telescope DOT. Since this step corrects pixel to pixel differences in sensitivity, the reduced spectra will be slightly noisier, although subsequent steps in the data reduction will mitigate it. In the wavelength calibration, we used a combination of arc lamps: Ne+Hg and He for TNG and Hg+Ar for DOT.

The next step is the sky subtraction. We took samples in each side of the object and fitted a polynomial of degree 1 or 2, when needed, and subtracted it from the spectra. After the sky subtraction, we used the fitted sky to check the wavelength calibration. We measured the wavelength of emission lines in the fitted sky background. In the objects where we found a constant offset between the measured and the reference value, we subtracted it from the wavelength solution.

Afterwards, we did the combination and extraction of the spectra and the flux calibration. Some objects improved their signal to noise ratio when reversing the order, extracting first and combining in the end. For the flux calibration, we observed spectrophotometric standard stars in each night of observation. We also corrected the atmospheric extinction at the observatory and the Galactic extinction with the values  $R=3.1$  and  $E(B - V)$  described in Table 1 (Schlafly & Finkbeiner 2011).

## 4 RESULTS

The reduced spectrum of one of the targets is shown in Figure 2, whereas, the remaining are presented in different figures in Appendix A. We have also plotted the normalized spectrum, which is calculated by fitting the continuum with a cubic spline function and dividing the spectrum by the fitted continuum. The spectra were scanned to identify emission/absorption lines to estimate the source redshift. For a consistency check, we also inspected the individual exposures and verified whether lines are visible in all of them. Altogether, the redshifts were measured for 11 BCUs out of 27 sources. Following the conventional emission line EW-based blazar classification scheme, 8 objects are identified as FSRQs ( $EW > 5\text{\AA}$ ). The spectra of 2 BL Lac sources were found to be dominated by the absorption features arising from the host galaxy, e.g., Ca II H&K doublet, allowing us to determine their redshifts. We tentatively identified the Ly- $\alpha$  absorption feature in the low-S/N optical spectrum of the candidate high-redshift BL Lac source 4FGL J1330.4+3157 and derived the source redshift to be  $z = 2.01$ . On the other hand, the featureless optical spectra of the remaining 16 BCUs imply that they can be classified as BL Lac objects. We discuss our findings about individual sources in the next section.

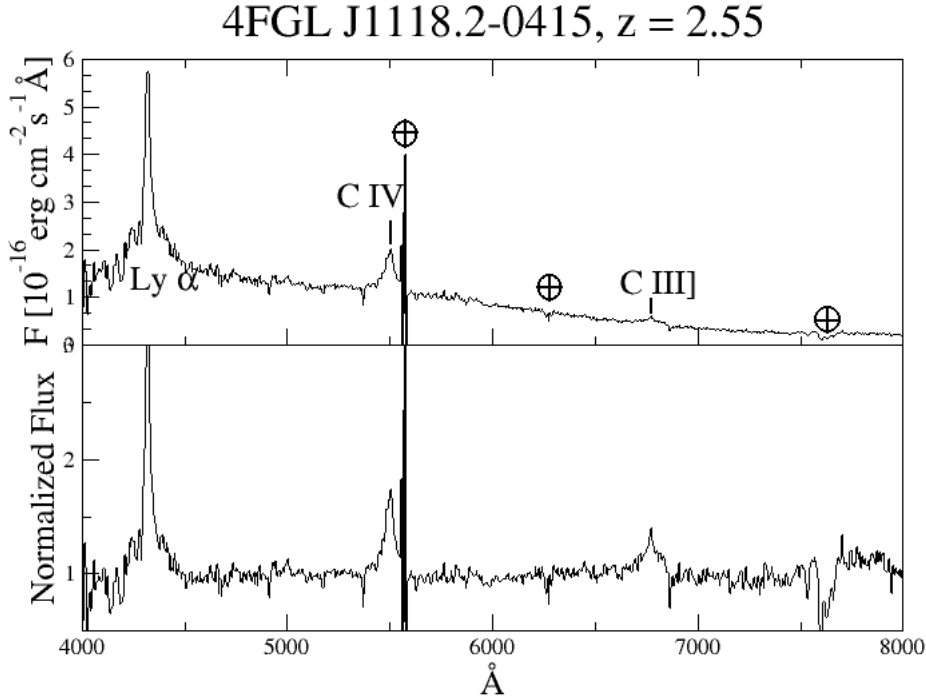


**Figure 2.** Optical spectrum of the BCU 4FGL J1118.2–0415 taken with the DOT. Top panel shows the observed spectrum whereas the normalized spectrum is shown in the bottom panel. Absorption/emission lines are highlighted.  $\oplus$  symbol indicates the position of sky emission and telluric absorption features.

## 5 NOTES ON INDIVIDUAL OBJECTS

*4FGL J0024.4+4647:* The spectrum is characterized by a blue continuum and four emission lines, Ly- $\alpha$  ( $EW_{\text{obs}}=148$  Å), Si IV ( $EW_{\text{obs}}=18.61$  Å), C IV ( $EW_{\text{obs}}=62.05$  Å), and C III ( $EW_{\text{obs}}=21.2$  Å), were identified. The derived redshift is 1.91 and the source can be classified as a FSRQ.

*4FGL J0028.9+3553, 4FGL J0130.6+1844, 4FGL J0223.5+3912, 4FGL J0233.5+0654:* The spectra of these BCUs are characterized by a blue continuum. No emission or absorption lines have been identified, implying them to be classified as BL Lac objects.

*4FGL J0244.7+1316:* The spectrum is characterized by a blue continuum. The emission lines Mg II ( $EW_{\text{obs}}=34.23$  Å) and [Ar IV] ( $EW_{\text{obs}}=5.8$  Å) are identified. The derived redshift is 0.98 and the source can be classified as a FSRQ.

*4FGL J0421.0–0752:* The spectrum is characterized by a red continuum and faint absorption features typically seen in the optical spectrum of elliptical galaxies, such as Ca II K ( $EW_{\text{obs}}=4.46$  Å), Ca II H ( $EW_{\text{obs}}=2.88$  Å), G-band ( $EW_{\text{obs}}=5.38$  Å), and Mg I ( $EW_{\text{obs}}=6.02$  Å), are observed. It is a BZG, a BL Lac with a host galaxy dominated spectrum.

*4FGL J0430.3+1654, 4FGL J0526.3+2246:* No emission/absorption lines are identified in the spectra of these BCUs. They can be categorized as BL Lac objects.

*4FGL J0604.9+0000:* The spectrum shows strong absorption lines Ca II K ( $EW_{\text{obs}}=2.24$  Å), Ca II H ( $EW_{\text{obs}}=0.83$  Å), H $\delta$  ( $EW_{\text{obs}}=2.74$  Å), G-band ( $EW_{\text{obs}}=101.47$  Å), and Mg I ( $EW_{\text{obs}}=105.80$  Å), characteristic of an elliptical galaxy. The redshift measured is  $z = 0.30$ . It is possibly a BZG, a BL Lac with host galaxy dominated spectrum.

*4FGL J0638.2+6020, 4FGL J0704.7+4508:* The spectrum is char-

acterized by red and blue continua, respectively, and no emission or absorption lines have been identified, implying these BCUs to be classified as BL Lac objects.

*4FGL J0746.5–0710:* The spectrum is characterized by a red continuum and faint emission lines. The broad emission line Mg II ( $EW_{\text{obs}}=16.92$  Å) is identified, leading to a source redshift of 0.90 and enabling the source to be classified as a FSRQ.

*4FGL J0749.6+1324:* The spectrum is characterized by several emission lines: C III ( $EW_{\text{obs}}=243.5$  Å), Mg II ( $EW_{\text{obs}}=289.1$  Å), and [Ne III] ( $EW_{\text{obs}}=48.34$  Å). The derived source redshift is 1.05 and the object can be classified as a FSRQ.

*4FGL J0804.5+0414, 4FGL J0929.6+4621:* The spectra are characterized by featureless continua. Accordingly, both sources can be classified as BL Lac objects.

*4FGL J0959.6+4606:* The spectrum is characterized by several faint absorption and narrow emission lines: G-band ( $EW_{\text{obs}}=8.9$  Å), [O III] ( $EW_{\text{obs}}=5.88$  Å), Mg I ( $EW_{\text{obs}}=6.09$  Å), and Na-D ( $EW_{\text{obs}}=4.93$  Å). Interestingly, the equivalent width of the [O III]5007 Å line is larger than 5 Å, indicating this source to be likely a FSRQ at redshift  $z = 0.14$ .

*4FGL J1118.2-0415:* The spectrum is characterized by a blue continuum and strong emission lines: Ly- $\alpha$  ( $EW_{\text{obs}}=95.46$  Å), C IV ( $EW_{\text{obs}}=26.54$  Å), and C III ( $EW_{\text{obs}}=8.11$  Å). The object can be classified as a FSRQ at the redshift of 2.55. This is the most distant blazar observed in our sample.

*4FGL J1129.2-0529:* The spectrum is featureless and the BCU can be classified as a BL Lac object.

*4FGL J1330.4+3157:* An absorption trough at  $\sim 3700$  Å is seen in the optical spectrum of this candidate high-redshift BL Lac object,

**Table 2.** Table with the emission/absorption lines identified in each spectrum. Column information are as follows: (1) 4FGL source name; (2) redshift derived from the identified lines; and (3) name of the identified lines.

4FGL Name (1)	Redshift (2)	Classification (3)	Lines identified (4)
J0024.4+4647	1.91	FSRQ	Ly- $\alpha$ , Si iv, C iv, C iii
J0028.9+3553		BL Lac	
J0130.6+1844		BL Lac	
J0223.5+3912		BL Lac	
J0233.5+0654		BL Lac	
J0244.7+1316	0.98	FSRQ	Mg iv, [Ar iv]
J0421.0-0752	0.28	BL Lac	Ca ii H & K, G band, Mg i
J0430.3+1654		BL Lac	
J0526.3+2246		BL Lac	
J0604.9+0000	0.30	BL Lac	Ca ii H & K, H $\delta$ , G-band, Mg i
J0638.2+6020		BL Lac	
J0704.7+4508		BL Lac	
J0746.5-0710	0.89	FSRQ	Mg ii
J0749.6+1324	1.05	FSRQ	C iii, Mg ii, [Ne iii]
J0804.5+0414		BL Lac	
J0929.6+4621		BL Lac	
J0959.6+4606	0.14	FSRQ	G-band, [O iii], Mg i, Na-D
J1118.2-0415	2.55	FSRQ	Ly- $\alpha$ C iv, C iii
J1129.2-0529		BL Lac	
J1330.4+3157	2.01	BL Lac	Ly- $\alpha$
J1419.4-0838	0.90	FSRQ	Mg ii
J1549.3+6310		BL Lac	
J1756.9+1531		BL Lac	
J1822.0+1600	0.98	FSRQ	C iii, Mg ii, [O ii], H $\epsilon$
J1836.5+1948		BL Lac	
J1845.0+1613		BL Lac	
J1949.0+1314		BL Lac	

which we interpret as Lyman- $\alpha$  absorption. Accordingly, the derived source redshift is  $z = 2.01$  thereby making it one of the very few  $z > 2$   $\gamma$ -ray detected BL Lac objects. A faint emission bump-like feature was also seen at  $\sim 4400$  Å which could be due to C iv emission supporting the source redshift of  $z = 2.01$ . However, a strong claim cannot be made due to the faintness of the target. Observations from larger telescopes will be needed to better constrain the redshift.

*4FGL J1419.4-0838*: The spectrum is characterized by a blue continuum and a strong Mg ii ( $EW_{\text{obs}}=40.72$  Å) emission line. The object can be classified as a FSRQ at the redshift of 0.90.

*4FGL J1549.3+6310*, *4FGL J1756.9+1531*: The spectra are characterized by featureless continua. Accordingly, the sources can be classified as BL Lac objects.

*4FGL J1822.0+1600*: The spectrum is characterized by a blue continuum and strong emission lines: C iii ( $EW_{\text{obs}}=19.48$  Å), Mg ii ( $EW_{\text{obs}}=27.8$  Å), [O ii] ( $EW_{\text{obs}}=5.93$  Å), and H $\epsilon$  ( $EW_{\text{obs}}=3.06$  Å). The object can be classified as a FSRQ at the redshift of 0.98.

*4FGL J1836.5+1948*, *4FGL J1845.0+1613*, *4FGL J1949.0+1314*: The spectra of these BCUs are characterized by featureless continua. Accordingly, they can be classified as BL Lac objects.

## 6 CONCLUSIONS

In this article, we have presented our findings based on the observations of 27  $\gamma$ -ray detected blazar candidates with the primary objective of measuring their redshift. We focused primarily on the LSP BCUs since almost all known broad emission line blazars are LSP sources and identifying emission lines in this class of objects

is relatively easier and less telescope time consuming compared to BL Lac objects. Out of 27 sources, we found broad emission lines in 8 BCUs and narrow emission/absorption features in 2 objects. In our sample, there are 4 sources with redshifts  $> 1$ . We admit that using only synchrotron peak frequency information may not be the only criterion to select potential broad-line blazars among the sample of *Fermi*-BCUs. Therefore, during upcoming observing runs within this long-term project, we will also consider other observational features, such as the location in the Wide-field Infrared Survey Explorer color-color diagram (cf. [Massaro et al. 2012](#)) and Compton dominance information ([Paliya et al. 2021](#)). These extra conditions would enable us to choose targets having a larger probability of exhibiting broad emission lines.

## ACKNOWLEDGEMENTS

We are grateful to the journal referee for constructive criticism. Part of the data presented herein was obtained at the Devasthal Optical Telescope (DOT), which is operated by Aryabhata Research Institute of Observational Sciences (ARIES). We thank the staff of ARIES who made these observations possible. Based on observations made with the Italian Telescopio Nazionale Galileo (TNG) operated by the Fundación Galileo Galilei (FGG) of the Istituto Nazionale di Astrofisica (INAF) at the Observatorio del Roque de los Muchachos (La Palma, Canary Islands, Spain). We thank the TNG telescope staff for the observations done in service mode. A.O.G. acknowledges financial support from the Spanish Ministry of Science, Innovation and Universities (MCIUN) under grant numbers RTI2018-096188-B-I00, and



from the Comunidad de Madrid Tec2Space project S2018/NMT-4291. A.D. acknowledges the support of the Ramón y Cajal program from the Spanish MINECO. P.S.-B acknowledges financial support from the Spanish Ministry of Science, Innovation and Universities (MCIUN) under grant number PID2019-107427GB-C31.

#### DATA AVAILABILITY

The spectra from this article can be found at <https://www.ucm.es/blazars/BCUs>.

#### REFERENCES

- Abdollahi S., et al., 2020, *ApJS*, **247**, 33
- Ackermann M., et al., 2011, *ApJ*, **743**, 171
- Ajello M., et al., 2012, *ApJ*, **751**, 108
- Ajello M., et al., 2020, *ApJ*, **892**, 105
- Álvarez Crespo N., et al., 2016, *AJ*, **151**, 95
- Bernieri E., Campana R., Massaro E., Paggi A., Tramacere A., 2013, *A&A*, **551**, L5
- Campana R., Massaro E., Bernieri E., D’Amato Q., 2015, *Ap&SS*, **360**, 19
- Chiaro G., Kovacevic M., La Mura G., 2021, *Journal of High Energy Astrophysics*, **29**, 40
- Condon J. J., Cotton W. D., Greisen E. W., Yin Q. F., Perley R. A., Taylor G. B., Broderick J. J., 1998, *AJ*, **115**, 1693
- Desai A., Marchesi S., Rajagopal M., Ajello M., 2019a, *ApJS*, **241**, 5
- Desai A., Helgason K., Ajello M., Paliya V., Domínguez A., Finke J., Hartmann D., 2019b, *ApJ*, **874**, L7
- Doert M., Errando M., 2014, *ApJ*, **782**, 41
- Domínguez A., et al., 2019, *ApJ*, **885**, 137
- Fermi-LAT Collaboration et al., 2018, *Science*, **362**, 1031
- Franceschini A., Foffano L., Prandini E., Tavecchio F., 2019, *A&A*, **629**, A2
- Hassan T., Dominguez A., Lefaucheur J., Mazin D., Pita S., Zech A., Consortium C., 2017, in 35th International Cosmic Ray Conference (ICRC2017), p. 632 ([arXiv:1708.07704](https://arxiv.org/abs/1708.07704))
- Kang S.-J., Fan J.-H., Mao W., Wu Q., Feng J., Yin Y., 2019, *ApJ*, **872**, 189
- Klindt L., van Soelen B., Meintjes P. J., Väisänen P., 2017, *MNRAS*, **467**, 2537
- Kovačević M., Chiaro G., Cutini S., Tosti G., 2020, *MNRAS*, **493**, 1926
- Landoni M., et al., 2015, *AJ*, **149**, 163
- Lyke B. W., et al., 2020, *ApJS*, **250**, 8
- Marchesi S., Kaur A., Ajello M., 2018, *AJ*, **156**, 212
- Marchesini E. J., et al., 2019, *Ap&SS*, **364**, 5
- Massaro F., D’Abrusco R., Tosti G., Ajello M., Gasparrini D., Grindlay J. E., Smith H. A., 2012, *ApJ*, **750**, 138
- Massaro F., Landoni M., D’Abrusco R., Milisavljevic D., Paggi A., Masetti N., Smith H. A., Tosti G., 2015, *A&A*, **575**, A124
- Massaro F., Marchesini E. J., D’Abrusco R., Masetti N., Andruchow I., Smith H. A., 2017, *ApJ*, **834**, 113
- Mattox J. R., et al., 1996, *ApJ*, **461**, 396
- Nievas Rosillo M., Domínguez A., Chiaro G., La Mura G., Brill A., Paliya V. S., 2022, *MNRAS*, **512**, 137
- Omar A., Yadav R. K. S., Shukla V., Mondal S., Pant J., 2012, in McLean I. S., Ramsay S. K., Takami H., eds, Society of Photo-Optical Instrumentation Engineers (SPIE) Conference Series Vol. 8446, Ground-based and Airborne Instrumentation for Astronomy IV. p. 844614, [doi:10.1117/12.925841](https://doi.org/10.1117/12.925841)
- Paggi A., et al., 2014, *AJ*, **147**, 112
- Paiano S., Falomo R., Franceschini A., Treves A., Scarpa R., 2017, *ApJ*, **851**, 135
- Paiano S., Falomo R., Treves A., Franceschini A., Scarpa R., 2019, *ApJ*, **871**, 162
- Paiano S., Treves A., Franceschini A., Falomo R., 2021, *MNRAS*, **508**, 6128
- Paliya V. S., Marcotulli L., Ajello M., Joshi M., Sahayanathan S., Rao A. R., Hartmann D., 2017, *ApJ*, **851**, 33
- Paliya V. S., Ajello M., Cao H. M., Giroletti M., Kaur A., Madejski G., Lott B., Hartmann D., 2020a, *ApJ*, **897**, 177
- Paliya V. S., Böttcher M., Olmo-García A., Domínguez A., Gil de Paz A., Franckowiak A., Garrappa S., Stein R., 2020b, *ApJ*, **902**, 29
- Paliya V. S., et al., 2020c, *ApJ*, **903**, L8
- Paliya V. S., Domínguez A., Ajello M., Olmo-García A., Hartmann D., 2021, *ApJS*, **253**, 46
- Pasham D. R., Wevers T., 2019, *Research Notes of the American Astronomical Society*, **3**, 92
- Peña-Herazo H. A., et al., 2019, *Ap&SS*, **364**, 85
- Rajagopal M., Marchesi S., Kaur A., Domínguez A., Silver R., Ajello M., 2021, *ApJS*, **254**, 26
- Saldana-Lopez A., Domínguez A., Pérez-González P. G., Finke J., Ajello M., Primack J. R., Paliya V. S., Desai A., 2021, *MNRAS*, **507**, 5144
- Schlafly E. F., Finkbeiner D. P., 2011, *ApJ*, **737**, 103
- Sol H., et al., 2013, *Astroparticle Physics*, **43**, 215
- Stickel M., Padovani P., Urry C. M., Fried J. W., Kuehr H., 1991, *ApJ*, **374**, 431
- Voges W., et al., 1999, *A&A*, **349**, 389
- van Dokkum P. G., 2001, *PASP*, **113**, 1420

#### APPENDIX A: OPTICAL SPECTRA

Here we show the optical spectra of all *Fermi*-BCUs observed with TNG and DOT.

This paper has been typeset from a  $\text{\TeX}/\text{\LaTeX}$  file prepared by the author.

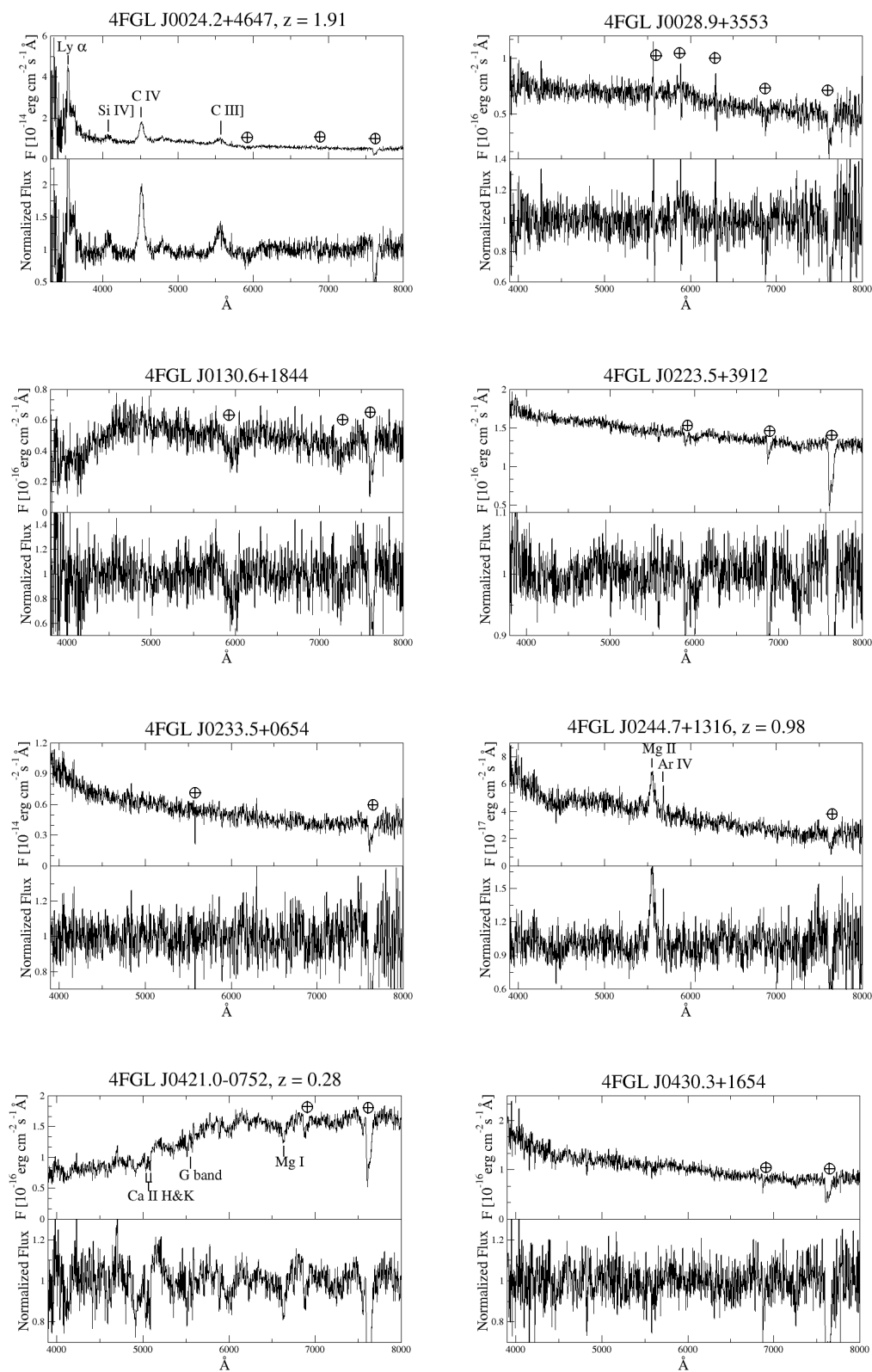


Figure A1. Same as Figure 2

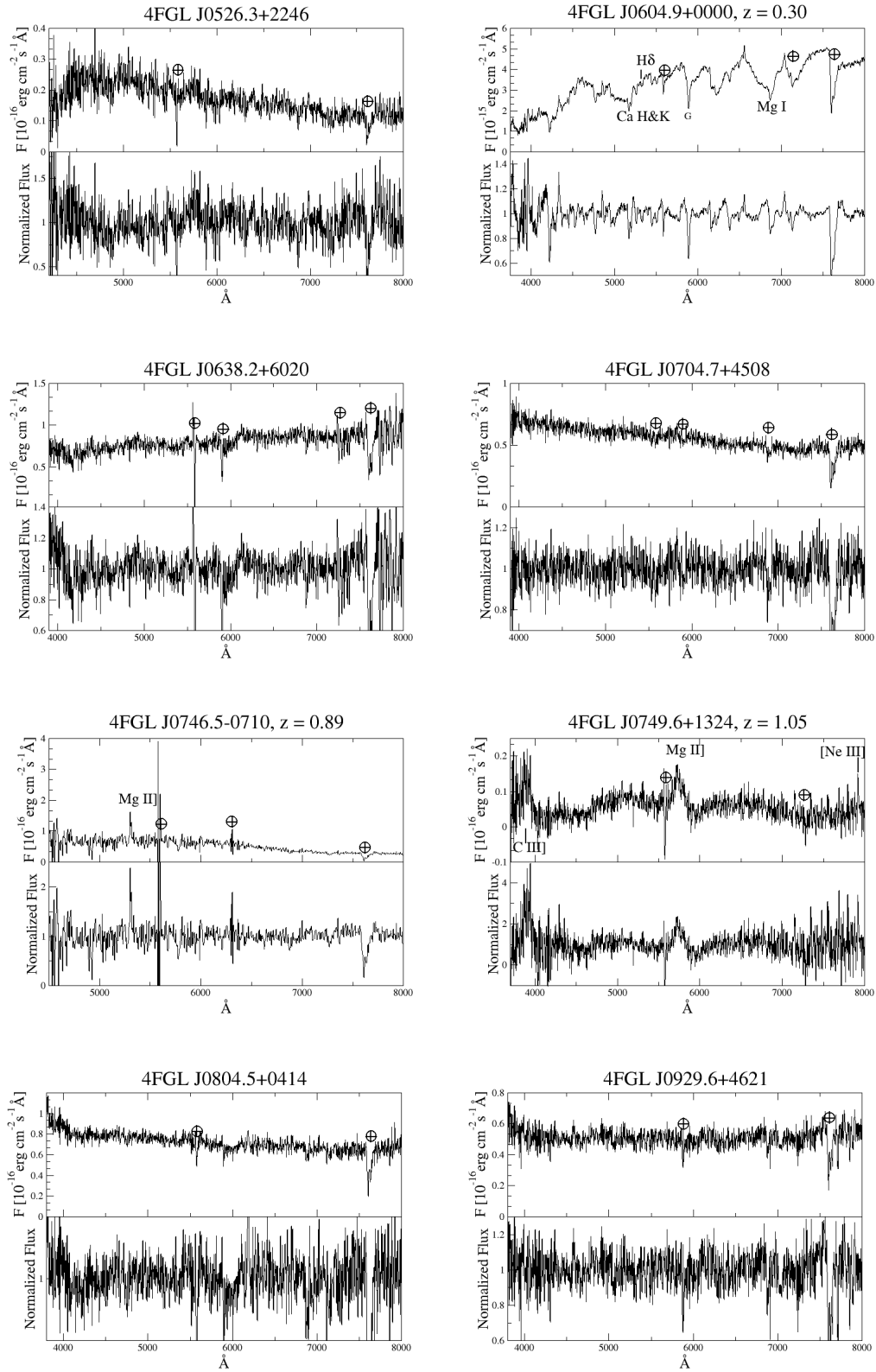


Figure A2. Same as Figure 2.



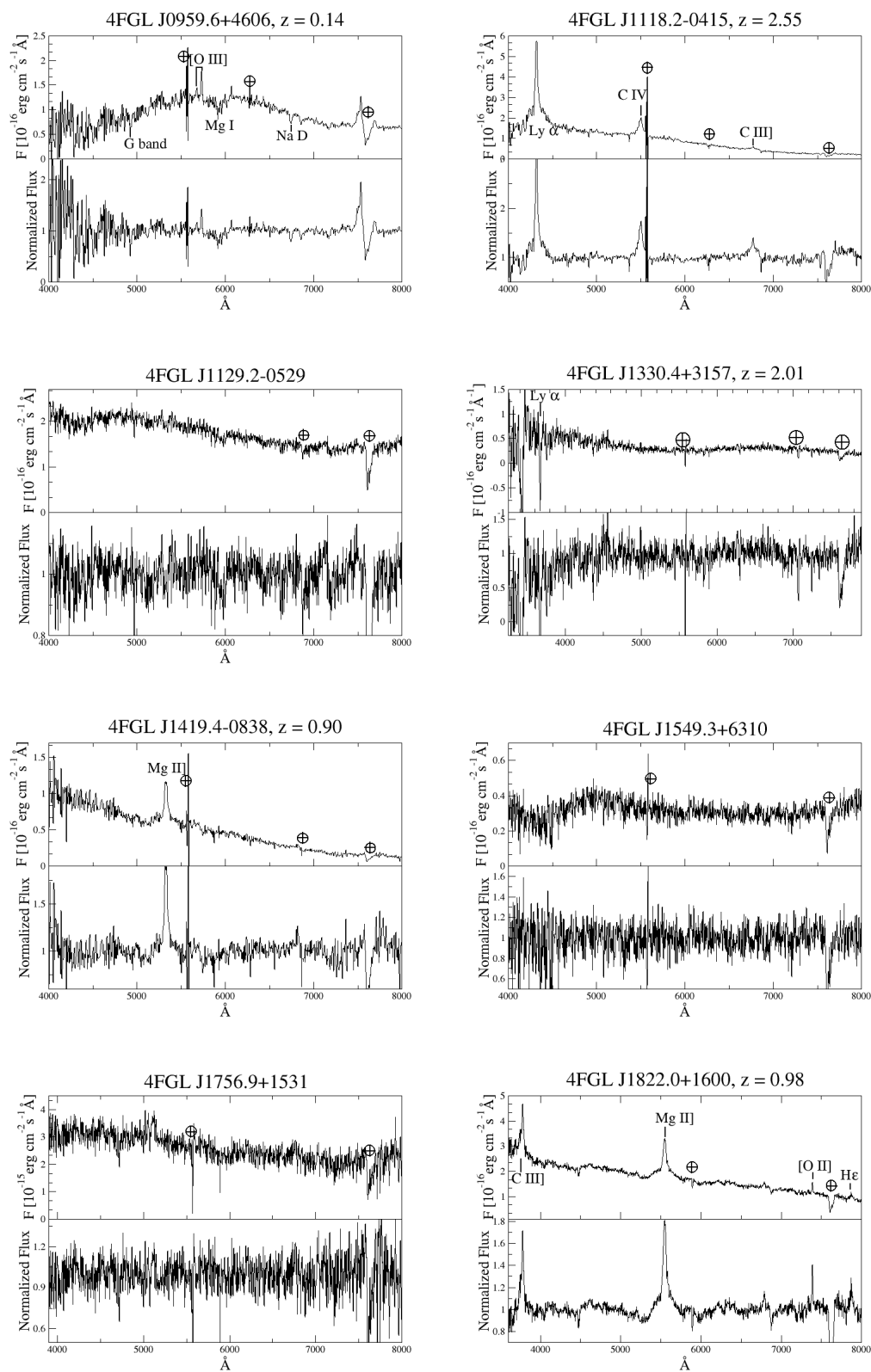
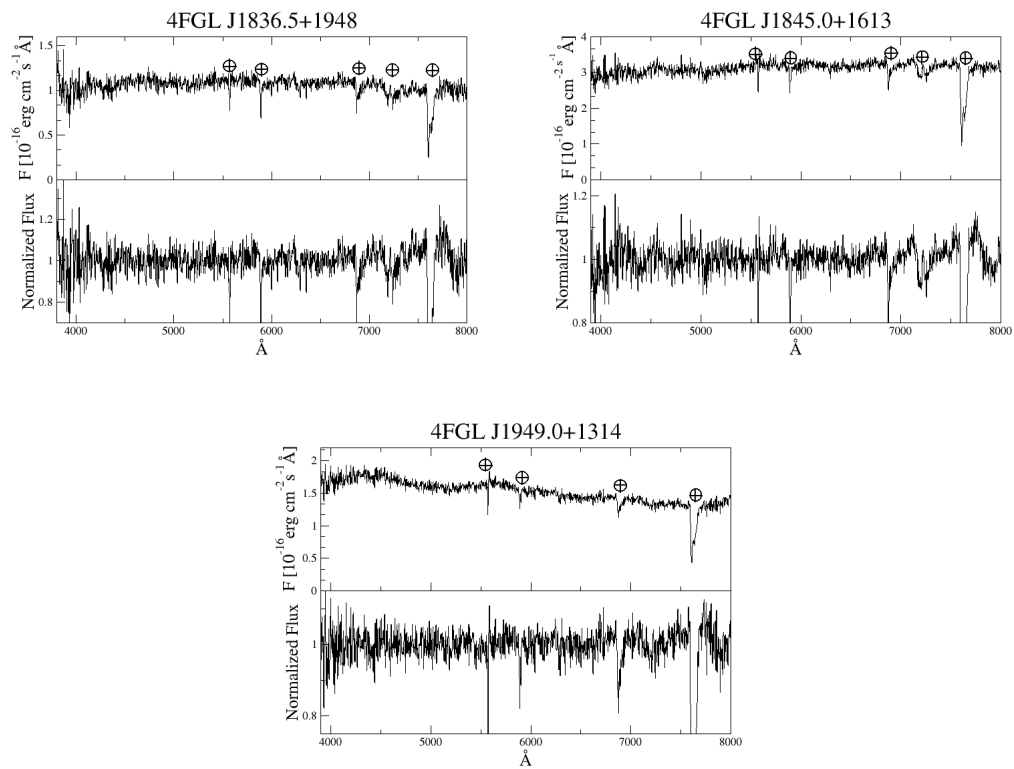


Figure A3. Same as Figure 2.



**Figure A4.** Same as Figure 2.